GEOPHYSICAL RESEARCH LETTERS, VOL. 34, L17802, doi:10.1029/2007GL031034, 2007

Seasonal variation in the correlation of airglow temperature and emission rate

P. J. Espy,[1] J. Stegman,[2] P. Forkman,[3] and D. Murtagh[3]

Received 18 June 2007; revised 10 July 2007; accepted 25 July 2007; published 1 September 2007.

[1] The hydroxyl (OH) rotational temperature and band emission rate have been derived using year-round, ground-based measurements of the infrared OH nightglow from Sweden from 1991 to 2002. Recent work has suggested that, during the winter, all scales of dynamical variations of radiance and temperature arise from vertical motions, implying that the effective source concentrations of atomic oxygen are constant. The present data show correlations between temperature and radiance both during winter and summer that are consistent with those observed in that previous work. However, during the transition to summer there is a rapid decrease in the temperature and its variation that is not reflected in the band radiance, suggesting that only the shorter-scale variations are accompanied by significant vertical motion. This indicates that the shorter-scale dynamical variations occur against an independent, seasonally changing background temperature profile in a way that is consistent with that predicted by gravity-wave models. **Citation:** Espy, P. J., J. Stegman, P. Forkman, and D. Murtagh (2007), Seasonal variation in the correlation of airglow temperature and emission rate, *Geophys. Res. Lett.*, *34*, L17802, doi:10.1029/2007GL031034.

1. Introduction

[2] Atmospheric gravity waves, with spatial scales of ten to a few hundred kilometers and temporal scales between five minutes and several hours, are typically generated in the lower atmosphere through the action of weather systems or orographic lifting of air masses [*Fritts and Alexander*, 2003, and references therein]. These waves grow in amplitude as they propagate into the rarified mesosphere, where wave motions vertically displace air parcels by several kilometers. The associated pressure disturbance perturbs the ambient airglow emission intensity and altitude, creating changes that may be monitored by ground-based instrumentation [*Swenson and Gardner*, 1998].

[3] Several space-borne measurements of airglow have found correlations between the airglow emission rate and altitude [*Ward et al.*, 1994; *Yee et al.*, 1997; *Liu and Shepherd*, 2006], which has been attributed to the vertical motions associated with large-scale atmospheric tides [*Zhang et al.*, 2001]. Similarly, recent ground-based work by *Cho and Shepherd* [2006] has shown that the OH nightglow displays a strong correlation between the derived rotational temperature and the band emission rate during the high-latitude winter. This correlation holds for 15-minute averages over the course of a day, as well as for daily-averaged values over an entire winter, and similar correlations are found for each of several winters. Using the dynamical model of *Ward* [1999], they conclude that the common process for airglow perturbations on all scales, including seasonal, is vertical motion, whereby downward motion produces heating, higher atomic oxygen mixing ratios and enhanced airglow emission.

[4] *Cho and Shepherd* [2006] point out that for vertical motions to control the relationship between radiance and temperature, the effective source concentrations of atomic oxygen should be constant at some altitude. However, their observations were confined to the winter season and do not reflect the range of dynamical and solar-flux conditions to which the mesosphere is subject over the course of the year. To test this hypothesis over different seasonal conditions, we have examined the correlation between the OH nightglow band emission rate and its derived rotational temperature over the full yearly cycle. Using near-infrared spectral measurements of the OH nightglow allowed observations during the polar summer so that this relationship could be examined as mesospheric winds shifted from wintertime, downward, to summertime, upward, conditions.

2. Instrumentation and Observations

[5] Michelson interferometer observations of the OH Meinel (3, 1) band nightglow were made in the spectral region between 1000 and 1700 nm at ~0.5 nm resolution in order to measure the OH radiance and to derive its rotational temperature. The measurements were made from Stockholm, Sweden (59.5°N, 18.2°E) during the summers of 1991 and 1993, and then continuously from 1993 through 1998. After 1998, the instrument was moved to Onsala, Sweden (57.4°N, 11.9°E) and continued data collection through 2002. Operating in the near infrared and in a semi-autonomous mode allowed continuous OH radiance and temperature measurements to be obtained whenever the sun was more than 5° below the horizon.

[6] The interferometer scanned each interferogram in ~3 seconds, but added scans in memory to yield an integration period of between ~5 and ~15 minutes for each spectrum, depending upon the radiance levels. Both a 1000 K blackbody and transfer standard were used to generate the spectral responses, and the OH line positions of *Maillard et al.* [1976] were used to calibrate the wavelength scales. Details of these spectral and wavelength calibrations are described by *Espy and Stegman* [2002].

[1]Physical Sciences Division, British Antarctic Survey, National Environment Research Council, Cambridge, UK.
[2]Department of Meteorology, Stockholm University, Stockholm, Sweden.
[3]Department of Radio and Space Science, Chalmers University of Technology, Göteborg, Sweden.

0094-8276/07/2007GL031034$05.00

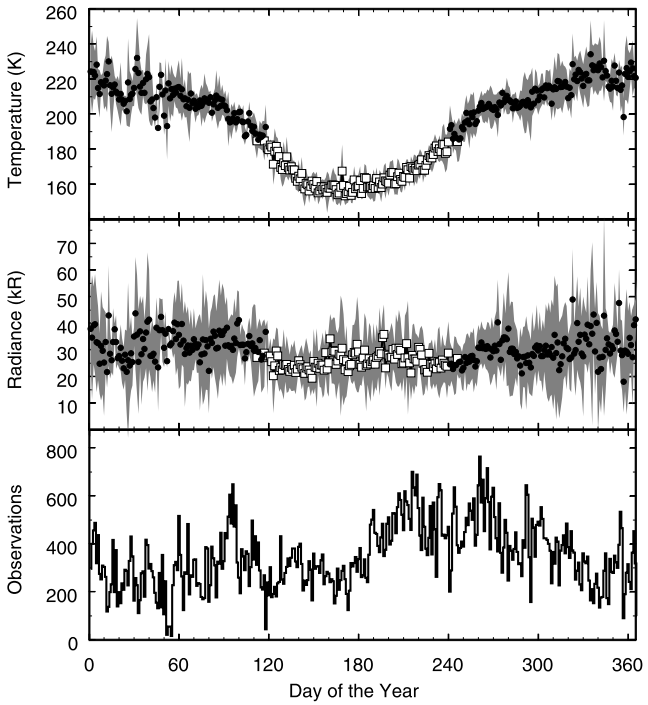

Figure 1. Nightly (top) hydroxyl airglow temperature and (middle) radiance level averaged over the years 1991–2002. The open symbols in both plots are those data with temperatures below 185 K and represent the summer season. The shaded regions show the standard deviation of the associated quantity over the time period. For those days with only a single year of data (5 nights), the standard deviation over the course of the night is displayed. (bottom) Number of individual 5–15 minute, cloud-free observations each day that were used to create the average quantities in the top and middle plots.

[7] *Espy et al.* [1995] describe in detail the spectral fitting technique used on the data. In brief, the spectral region containing the P, Q and R branches of the (3, 1) Meinel vibration-rotation band was synthesized by convolving the instrumental line-shape function with the line strengths of *Mies* [1974], a Boltzmann model of the rotational-level population, and a model scattered solar spectrum [*Berk et al.*, 1989]. The rotational temperature, integrated band strength and a scaling for the solar scatter were then adjusted to give a best, least-squares fit to the data [*Hill et al.*, 1979]. In order to remove the contribution of continuum radiation, both the data and the model were high-pass filtered before fitting. Using a sample of data obtained under clear-sky conditions, as verified by an observer, the relative uncertainty estimates for the individual fits of integrated band radiance and rotational temperature were typically on the order of 1–3% and 3–5%, respectively. Data periods obscured by clouds were marked by a significantly reduced signal-to-noise, resulting in the fitting routine either failing to converge or converging with large uncertainty estimates. It was empirically determined that relative error estimates three-sigma larger than the clear-sky data were contaminated by cloud and dropped from the analysis.

[8] After processing, the individual 5 to 15 minute temperature and radiance values were combined to form a single nightly average. This averaging had the effect of smoothing out the variations caused by short-period gravity waves. However, during individual nights, the OH temperature can vary by 3–5%, and the radiance by as much as a factor of two, due to both photo-chemical and tidal effects [*Lowe et al.*, 1996]. Therefore, in order to prevent data gaps caused by cloudy periods during the night from skewing the average, nights with less than 100 minutes of data were discarded. On average, each daily mean consisted of 62 ± 30 individual measurements.

3. Analysis and Results

[9] The average annual cycles of the nightly averaged OH temperature and integrated volume emission rate in kR (hereafter referred to simply as radiance) are shown in the top and middle plots of Figure 1, respectively. The shaded regions in the top and middle plots illustrate the daily standard deviations of the associated quantities over the 12 years, and the bottom plot shows the number of cloud-free observations used each day. The primary seasonal variation results from the dynamical driving of the mesospheric circulation. The wintertime, downward winds result in compressional heating, and the summertime, upward conditions result in adiabatic cooling. This results in the decreases of ~45 K in temperature and 5 kR in radiance observed during the summer. The points at which the temperature drops rapidly from its average winter value are somewhat displaced from the equinoxes, creating a shorter, asymmetric summer season [*Espy and Stegman*, 2002]. Since these coincide with an average temperature of ~185 K, data with temperatures at or below this are taken to be summer data and are shown by the open symbols in Figure 1 and all subsequent figures.

[10] In Figure 2, the individual nightly averaged temperatures are plotted against the corresponding radiances for the years between 1991 and 2002. The error bars shown at the top of Figure 2 represent the average uncertainty in temperature and radiance for the nightly averages. Accordingly, the radiance is taken as the independent variable due to its smaller statistical uncertainty. The summer and winter data show distinct differences in their relationship between temperature and radiance. The winter data show a linear correlation that is consistent over the 12 years of data, confirming and extending the results of *Cho and Shepherd* [2006]. The summer data, whilst displaying a consistent year-to-year linear correlation, exhibit a slope that is significantly flatter than that of the winter data. The linear fits, weighted by the temperature standard deviations, are 0.36 ± 0.03 K/kR for winter, and 0.13 ± 0.04 K/kR for summer. The 90% confidence boundaries for each fit, indicated by the dashed lines in Figure 2, encompass the bulk of the respective data points without overlap, highlighting the independent behaviour of the two populations. The slope reduction indicates that there is a smaller temperature change for a given radiance variation during summer. In addition, the nearly vertical displacement of the curve downward during summer indicates that the seasonal transition does not follow the intra-seasonal relationship between temperature and radiance.

[11] The temperature scatter within the populations in Figure 2 reflects not only the year-to-year variability, but

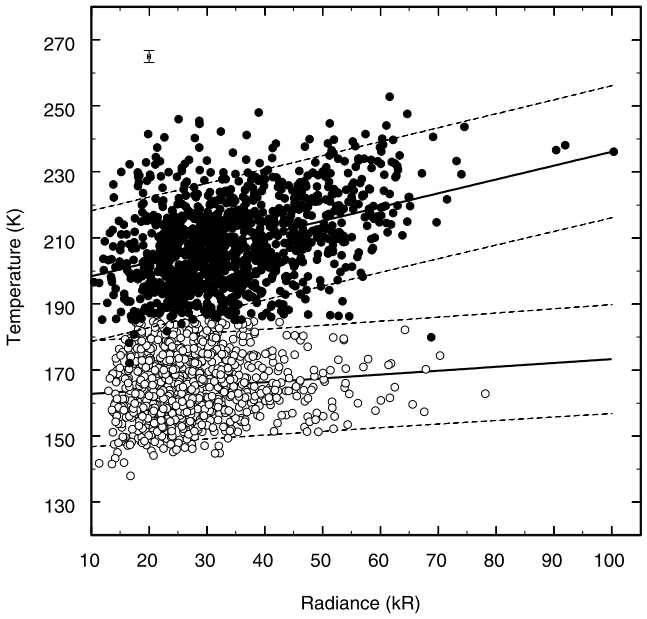

Figure 2. Scatter plot of temperature versus emission rate for the individual nightly averaged observations of the OH Meinel (3,1) band from 1991–2002. The open symbols in both plots are those data with temperatures below 185 K and represent the summer season, while the closed symbols show the winter data. The error bars in the upper left-hand corner indicate the averaged standard error of the mean of all observations, and the individual errors were used to weight the linear regressions that are shown by the solid curves. The dashed lines show the 90% confidence intervals for these fits.

also changes associated with the transition between the winter and summer conditions noted above. To gauge the importance of each, the nightly averages for single months around solstice can be examined. In Figure 3, the individual nightly averaged temperatures are plotted against the corresponding radiances for all the December and June data between 1991 and 2002. Immediately apparent is the reduced scatter in the temperatures, even though the same time period of Figure 2 is represented. There is again a strong, year-to-year correlation between temperature and radiance, with the December data once more yielding the steeper gradient of 0.40 ± 0.07 K/kR, as compared to the June gradient of 0.20 ± 0.05 K/kR. In fact, the slope remains above 0.3 K/kR from September through May, and below 0.2 K/kR from June through August. Additionally, the December and June solstice data lie along the respective upper and lower confidence bands of the winter and summer populations, shown by the shaded regions in Figure 3. Thus, the shift in both slope and mean temperature during the transition between winter and summer, rather than the year-to-year variability, is the cause of the temperature scatter observed in Figure 2.

4. Summary and Conclusions

[12] The present work shows that the OH airglow temperature is strongly and consistently correlated with the band radiance over the 12 years of observations, confirming and extending the observations of *Cho and Shepherd* [2006]. These correlations occur during both summer and winter, suggesting that, within each season, the common process for airglow perturbations is most likely dynamically driven vertical motion. However, the slope of the relationship between the temperature and radiance (in K/kR) decreases by ~36% from the winter to summer season. In addition, the rapid change of temperature, ~45 K, during the seasonal transition is accompanied by only a ~5 kR change in radiance, resulting in the offset of the winter and summer curves shown in Figures 2 and 3.

[13] This offset indicates that the seasonal transition does not follow the intra-seasonal relationship between temperature and radiance. If the decreased summer radiances were produced by a large increase in the OH emission altitude and a corresponding cooling in accordance with the temperature-radiance relationships found here, the non-linear temperature dependence of the OH photochemistry could compensate by increasing the radiance at the lower temperatures. However, such a process would *increase* the summertime slope of the temperature-radiance relationship (in K/kR), since the photo-chemical radiance increase with decreasing temperature is largest in summer. Thus, the present observations cannot be explained by photochemistry alone. It would therefore appear that the seasonal transition may be accompanied by changes in the atomic oxygen source function, while the vertical motions associated with dynamical variations take place against a temperature profile that is relatively fixed by the mean vertical winds.

[14] *Swenson and Gardner* [1998] modelled gravity-wave variations of the OH radiance and temperature against

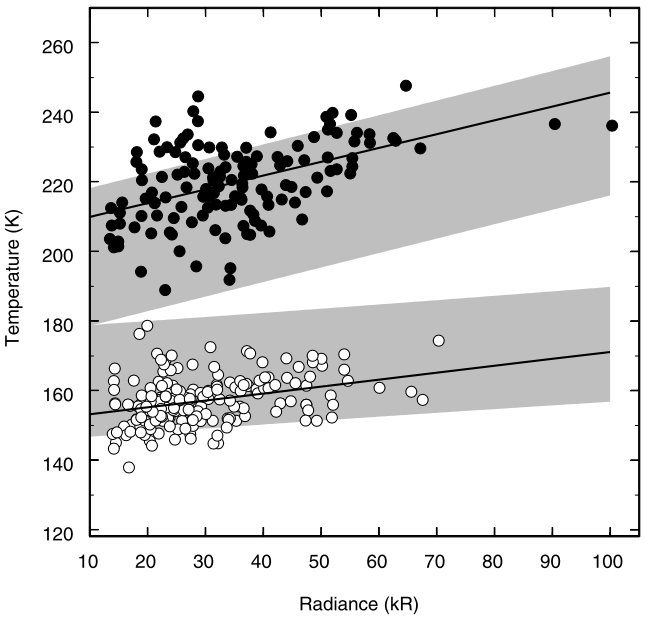

Figure 3. Scatter plot of temperature versus emission rate for the individual nightly averaged observations during all June (open symbols) and December (solid symbols) periods between 1991 and 2002. The solid lines show the linear regression fits, weighted by the individual uncertainties, and the shaded regions are the 90% confidence intervals of the entire summer and winter population regressions shown in Figure 2.

a fixed temperature profile. This work showed that while the relative OH radiance response to gravity waves of different vertical wavelengths is rather constant throughout the year, the relative temperature response is significantly smaller in summer than in winter due to the increased temperature lapse rate. They find that the effect on the temperature response is negligible only for lapse rates whose magnitude $\ll$4 K/km, which are typically found during winter. At mid latitudes, they show a 20% decrease in summer temperature response with a $\sim$2 K/km lapse rate. At high latitudes, where the magnitude of the lapse rate in the OH region can be $\sim$4 K/km [*Lübken et al.*, 1990], we observe 36% decrease in the temperature response in keeping with the model results. Thus, the decrease in slope of the radiance-temperature correlation during summer is consistent with the shorter time-scale variations of radiance and temperature within a season being caused by vertical motions associated with dynamical perturbations.

[15] We find that the correlation between OH radiance and temperature is consistent from year to year over the course of a solar cycle, supporting the hypothesis of *Cho and Shepherd* [2006] that the effective source concentrations of atomic oxygen are constant at some altitude year to year. However, in contrast to their assertion that airglow perturbations on all time scales, including seasonal, are caused by vertical motion, we do not find a continuous relationship between temperature and radiance for the seasonal variation. Rather, there is a large decrease in both temperature and its short-period variation from winter to summer that is not reflected in the radiance, resulting in a decreased slope and offset of the correlation curves. Thus, the seasonal variations, which are accompanied by only a $\sim$1 km change in emission altitude of the OH [*Liu and Shepherd*, 2006], occur independently and may be the result of seasonal changes in the atomic oxygen source function. They then represent a fixed background upon which the shorter-scale dynamical fluctuations then take place. The observed decrease in the temperature response during summer of these perturbations agrees with the model results of *Swenson and Gardner* [1998], adding further support to the hypothesis that these correlated short-period fluctuations are the result of vertical motions associated with dynamical perturbations [*Cho and Shepherd*, 2006; *Liu and Shepherd*, 2006].

[16] **Acknowledgments.** This work was jointly supported by US National Science Foundation grant ATM-9714933, the International Meteorological Institute of Stockholm University, the UK Natural Environment Research Council, and Swedish Natural Science Research Council grants G-AA/GU 04784-304 and 50427-001.

References

Berk, A., L. S. Bernstein, and D. C. Robertson (1989), MODTRAN: A moderate resolution model for LOWTRAN 7, *GL-TR-89-0122*, Air Force Geophys. Lab., Hanscom AFB, Mass.

Cho, Y.-M., and G. G. Shepherd (2006), Correlation of airglow temperature and emission rate at Resolute Bay (74.68°N), over four winters (2001–2005), *Geophys. Res. Lett.*, *33*, L06815, doi:10.1029/2005GL025298.

Espy, P. J., and J. Stegman (2002), Trends and variability of mesospheric temperature at high latitudes, *Phys. Chem. Earth*, *27*, 543–553.

Espy, P. J., R. Huppi, and A. Manson (1995), Large scale, persistent latitude structures in the mesospheric temperature during ANLC-93, *Geophys. Res. Lett.*, *22*, 2801–2804.

Fritts, D. C., and M. J. Alexander (2003), Gravity wave dynamics and effects in the middle atmosphere, *Rev. Geophys.*, *41*(1), 1003, doi:10.1029/2001RG000106.

Hill, R. A., A. J. Mulac, and D. P. Aeschliman (1979), Temperatures from rotational-vibrational Raman Q-branches, *J. Quant. Spectosc. Radiat. Transfer*, *21*, 213–220.

Liu, G., and G. G. Shepherd (2006), An empirical model for the altitude of the OH nightglow emission, *Geophys. Res. Lett.*, *33*, L09805, doi:10.1029/2005GL025297.

Lowe, R. P., L. M. LeBlanc, and K. L. Gilbert (1996), WINDII/UARS observations of twilight behaviour of the hydroxyl airglow, at mid latitude equinox, *J. Atmos. Terr. Phys.*, *58*, 1863–1869.

Lübken, F.-J., et al. (1990), Mean state densities, temperatures and winds during the MAC/SINE and MAC/EPSILON campaigns, *J. Atmos. Terr. Phys.*, *52*, 955–970.

Maillard, J. P., J. Chauville, and A. W. Mantz (1976), High-resolution emission spectrum of OH in an ocyacetylene flame from 3.7 to 0.9 μm, *J. Mol. Spectrosc.*, *63*, 120–141.

Mies, F. H. (1974), Calculated vibrational transition probabilities of OH ($X^2\Pi$), *J. Mol. Spectrosc.*, *53*, 150–188.

Swenson, G. R., and C. S. Gardner (1998), Analytical models for the responses of the mesospheric OH* and Na layers to atmospheric gravity waves, *J. Geophys. Res.*, *103*, 6271–6294.

Ward, W. E. (1999), A simple model of diurnal variations in the mesospheric oxygen nightglow, *Geophys. Res. Lett.*, *26*, 3565–3568.

Ward, W. E., Y. J. Rochon, C. McLandress, D. Y. Wang, J. R. Criswick, B. H. Solheim, and G. G. Shepherd (1994), Correlations between the mesospheric O(^{1}S) emission peak intensity and height and temperature at 98 km using WINDII data, *Adv. Space Res.*, *14*, 57–60.

Yee, J.-H., G. Crowley, R. G. Roble, W. R. Skinner, M. D. Burrage, and P. B. Hays (1997), The influence of the diurnal tide on the O(^{1}S), $O_2(^1\Sigma)$ and OH mesospheric nightglow emissions, *J. Geophys. Res.*, *102*, 19,949–19,968.

Zhang, S. P., R. G. Roble, and G. G. Shepherd (2001), Tidal influence on the oxygen and hydroxyl nightglows: Wind Imaging Interferometer observations and thermosphere/ionosphere/mesosphere electrodynamics general circulation model, *J. Geophys. Res.*, *106*, 21,381–21,393.

P. J. Espy, Physical Sciences Division, British Antarctic Survey, National Environment Research Council, High Cross, Madingley Road, Cambridge, CB3 0ET, UK.

P. Forkman and D. P. Murtagh, Department of Radio and Space Science, Chalmers University of Technology, SE-412 96 Göteborg, Sweden.

J. Stegman, Department of Meteorology, Stockholm University, SE-106 91 Stockholm, Sweden.